Received: 7 October 2022 | Revised: 6 March 2023 | Accepted: 13 March 2023

DOI: 10.1096/fj.202201623RR

RESEARCH ARTICLE

The FASEB Journal

CD93 maintains endothelial barrier function by limiting the phosphorylation and turnover of VE-cadherin

Roberta Lugano[1] | **Kalyani Vemuri**[1] | **Stefano Barbera**[1] | **Maurizio Orlandini**[2] | **Elisabetta Dejana**[1,3] | **Lena Claesson-Welsh**[1] | **Anna Dimberg**[1]

[1]Department of Immunology, Genetics and Pathology, Science for Life Laboratory, Uppsala University, The Rudbeck Laboratory, 75185, Uppsala, Sweden

[2]Department of Biotechnology, Chemistry and Pharmacy, University of Siena, Via A. Moro, 2, 53100, Siena, Italy

[3]Vascular Biology Unit, FIRC Institute of Molecular Oncology, Milan, 20129, Italy

Correspondence
Anna Dimberg and Roberta Lugano, Department of Immunology, Genetics and Pathology, Science for Life Laboratory, Uppsala University, The Rudbeck Laboratory, 75185 Uppsala, Sweden.
Email: anna.dimberg@igp.uu.se and roberta.lugano@igp.uu.se

Funding information
Barncancerfonden (Swedish Childhood Cancer Foundation), Grant/Award Number: PR2018-0148 and PR2021-0122; Cancerfonden (Swedish Cancer Society), Grant/Award Number: CAN 2017/502, 20 1008 PjF and 20 1010 UsF; Hjärnfonden (Brain Foundation), Grant/Award Number: FO2022-0366; Knut och Alice Wallenbergs Stiftelse (Knut and Alice Wallenberg Foundation), Grant/Award Number: KAW 2019.0088; Vetenskapsrådet (VR), Grant/Award Number: Dnr 2020-02563

Abstract

Regulation of vascular permeability to plasma is essential for tissue and organ homeostasis and is mediated by endothelial cell-to-cell junctions that tightly regulate the trafficking of molecules between blood and tissue. The single-pass transmembrane glycoprotein CD93 is upregulated in endothelial cells during angiogenesis and controls cytoskeletal dynamics. However, its role in maintaining homeostasis by regulating endothelial barrier function has not been elucidated yet. Here, we demonstrate that CD93 interacts with vascular endothelial (VE)-cadherin and limits its phosphorylation and turnover. CD93 deficiency in vitro and in vivo induces phosphorylation of VE-cadherin under basal conditions, displacing it from endothelial cell–cell contacts. Consistent with this, endothelial junctions are defective in CD93$^{-/-}$ mice, and the blood–brain barrier permeability is enhanced. Mechanistically, CD93 regulates VE-cadherin phosphorylation and turnover at endothelial junctions through the Rho/Rho kinase-dependent pathway. In conclusion, our results identify CD93 as a key regulator of VE-cadherin stability at endothelial junctions, opening up possibilities for therapeutic strategies directed to control vascular permeability.

KEYWORDS

blood–brain barrier, CD93, endothelial junctions, RhoGTPases, vascular permeability, VE-cadherin

1 | INTRODUCTION

The endothelial barrier maintains vascular and tissue homeostasis and is mainly mediated by cell-to-cell junctions that tightly regulate the transfer of large molecules and cells between the blood and the surrounding tissue. Dysregulated endothelial barrier and increased vascular permeability contribute to the progression of many pathological conditions including neurological diseases, cancer, and cardiovascular diseases among others and can influence treatment efficacy.[1] Thus, better understanding of the molecular mechanisms that cooperate in the control of vascular permeability may improve the development of new therapeutic interventions to limit endothelial barrier dysfunctions.

Endothelial junction complexes, adherens junctions (AJs), and tight junctions (TJs) play a pivotal role in maintaining the physical barrier in the blood vessels. These endothelial junction complexes are composed of highly specialized transmembrane molecules, such as cadherin and claudin family proteins, with vascular endothelial (VE)-cadherin, and claudin-5 being important components of the AJs and TJs, respectively.[2] Both junction types are structurally and functionally linked to the actin cytoskeleton through several adaptor molecules including catenins and zonula occludens (ZO) family members.[1] Therefore, intracellular signaling affecting actin dynamics is essential in regulating endothelial barrier function.[3,4] In this aspect, the RhoGTPase family members, Rac1, Cdc42, and RhoA, play critical roles in the regulation of the endothelial barrier by mediating actin cytoskeleton rearrangements.[5] Dismantling of endothelial junctions can be triggered by permeability-inducing agents such as vascular endothelial growth factor-A (VEGF-A), histamine, bradykinin, and other mediators, by promoting phosphorylation and internalization of the junctional proteins and by affecting actin cytoskeleton dynamics.[3,6]

In recent years, the C-type lectin transmembrane protein CD93 has been shown to play an important role in vascular biology. Our previous work identified CD93 within a subset of genes upregulated in high-grade glioma vasculature.[7] Moreover, CD93 has emerged as a potential target for anti-angiogenic therapy due to its inclusion as one of the top 20 genes in a core human primary tumor angiogenesis signature.[8] Consistent with its role in tumor angiogenesis, CD93 is predominantly expressed in endothelial cells and consists of an extracellular part including a C-type lectin domain, a sushi domain, five epidermal growth factor (EGF)-like repeats, a serine/threonine-rich mucin-like domain, a transmembrane domain, and a short cytoplasmic domain carrying a binding site for moesin that anchors CD93 to the cytoskeleton.[9]

We have previously demonstrated that in vitro silencing of CD93 is associated with actin cytoskeleton remodeling and that CD93 deficiency leads to increased tumor vascular permeability, impaired vessel perfusion, and maturation in in vivo model of glioma.[10,11] Furthermore, CD93-mediated endothelial cytoskeletal remodeling during cell adhesion and migration is dependent on RhoGTPase signaling.[12,13] While these findings emphasize the general involvement of CD93 in regulating endothelial function, its role in controlling the endothelial barrier properties during homeostasis has remained unexplored.

In this study, we investigated the contribution of CD93 in the regulation of endothelial junction stability through in vitro and in vivo CD93 loss-of-function approaches. Our data demonstrate that CD93 interacts with VE-cadherin and suppress its phosphorylation and internalization, thus preserving endothelial junction stability. CD93 deficiency displaces VE-cadherin and claudin-5 from endothelial cell–cell junctions. The disruption of VE-cadherin and claudin-5 in the absence of CD93 is rescued by inhibiting Rho signaling in endothelial cells, demonstrating that CD93 regulates endothelial barrier properties through a RhoA/Rho kinase-dependent pathway. Moreover, in vivo CD93 deficiency induces remodeling of endothelial junctions in the brain vasculature, compromising the endothelial barrier function. In conclusion, we identify CD93 as a key component in the maintenance of vascular integrity in physiological conditions by stabilizing VE-cadherin at the cell–cell junctions.

2 | MATERIALS AND METHODS

2.1 | Mice

CD93$^{-/-}$[14] and wild-type littermates were bred in house. C57Bl/6 wild-type mice were purchased from Taconic M&B (Bomholt, Denmark). All animal experiments in this study were performed in 10-week-old littermates mice. All animal experiments in this study were performed according to the guidelines for animal experimentation and welfare provided by Uppsala University and approved by the Uppsala County regional ethics committee (Dnr C1/14; C26/15; Dnr 5.8.18-19429/2019).

2.2 | Cells

Human dermal blood lymphatic free endothelial cells (HDBECs) isolated from juvenile foreskin (Cat# C-12211; PromoCell, Heidelberg, Germany) were cultured in gelatin-coated culture dishes in Endothelial Cell Basal Medium with full supplements (EBM-MV2,

PromoCell). Human brain microvascular endothelial cells (HBMVECs, iXCells Biotechnologies, 10HU-051) were cultured in collagen-coated culture dishes in EBM-MV2 medium. Cells were maintained at 37°C and 5% CO_2/95% air in a humidified chamber. Mycoplasma test was routinely performed in all cell cultures used in this study.

2.3 | Brain tissue collection and preparation

Mice were anesthetized and perfused by intracardiac injection of 10 mL of 1× phosphate-buffered saline (PBS) and 10 mL of 4% (wt/vol) paraformaldehyde (PFA) using a peristaltic pump (flow rate: 2 mL/min). After that, brains were excised, post-fixed in 4% PFA overnight at 4°C, dehydrated in 30% sucrose, and vibratome sectioned for immunofluorescent staining. Alternatively, for transmission electron microscopy (TEM) analysis, mice were perfused with 0.1 M sodium cacodylate buffer (pH 7.4) followed by fixation in 2.5% glutaraldehyde +1% PFA in 0.1 M sodium cacodylate buffer (pH 7.4). After perfusion, mice were kept in a sealed plastic bag at room temperature for 2 h. Brains were excised and stored at 4°C in the fixative buffer until further processed.

2.4 | Immunofluorescent staining

Vibratome sections (80 μm) from PFA-fixed cryoprotected brain tissues were air-dried and permeabilized in PBS containing 0.1% Triton-X100. Sections were blocked in PBS containing 3% BSA, and incubated with primary antibodies. The following primary antibodies were used: anti-CD31 (Cat# MA3105; clone 2H8; RRID: AB_223592; ThermoFisher Scientific, Massachusetts, USA), anti-claudin 5 (Cat# 34-1600; RRID: AB_2533157; ThermoFisher Scientific), anti-VE-cadherin (Cat# 555289; RRID: AB_395707; BD Biosciences, New Jersey, USA), anti-VE-cadherin pY658 and pY685,[15] anti-fibrinogen (A0080; RRID: AB_2894406; Dako, CA, USA), anti-vWF (A0082; RRID: AB_2315602, Dako, CA, USA), and Anti-actin α-smooth muscle-Cy3 (ACTA2; C6198; RRID: AB_476856, Sigma, MO USA). Sections were washed in PBS and stained with Alexa Fluor-conjugated secondary antibodies (ThermoFisher Scientific). Nuclei were stained with Hoechst 33342 (Sigma-Aldrich), and the sections were mounted using Fluoromount-G (Cat# 0100-01; Southern Biotech, Alabama, USA) and imaged under confocal microscope (SP8, Leica Microsystems, Wetzlar, Germany). A representative image of at least three individual immunofluorescent staining is shown.

siRNA-transfected HDBECs or HBMVECs were plated on eight-well chamber slides, grown until confluency and then fixed in 4% PFA. After permeabilization in 1% BSA/0.1% Triton-X100/PBS and blocking in 3% BSA/0.1% Tween-20/PBS, the cells were probed with primary antibodies VE-cadherin (Cat# 2500, RRID: AB_10839118; Cell Signaling, Massachusetts, USA), claudin-5 (Cat# 35-2500, RRID: AB_2533200, ThermoFisher Scientific), ZO-1 (61-7300, RRID: AB_2533938; ThermoFisher Scientific) diluted in blocking buffer at 4°C overnight, and incubated with appropriate Alexa Fluor-conjugated secondary antibodies (ThermoFisher Scientific) diluted in blocking buffer at room temperature for 2 h. Nuclei and actin were stained with Hoechst 33342 and Alexa Fluor 647-conjugated phalloidin, respectively (all from ThermoFisher Scientific). Subsequently, cells were washed with PBS, mounted with Fluoromount-G (Southern Biotech; 0100-01), and kept in 4°C for imaging. Cells were analyzed using a Leica SP8 confocal microscope (Leica Microsystems). A representative image of at least three independent immunofluorescent staining is shown.

2.5 | Transmission electron microscopy

Perfused-fixed brain samples were rinsed with 0.1 M sodium cacodylate buffer (pH 7.4) for 10 min prior to 1-h incubation in 1% osmium tetroxide/0.1 M sodium cacodylate buffer. After a further rinse in 0.1 M sodium cacodylate buffer, samples were dehydrated in graded alcohols (70%–99.9%) for a total of 1.5 h, followed by 5-min incubation in propylene oxide. Samples were then placed in a mixture of EPON resin and propylene oxide (1:1) for 1 h, followed by two changes of 100% resin, the first for 2–4 h and the last overnight. Subsequently, samples were embedded in capsules in newly prepared Epon resin and left for 1 h and then polymerized at 60°C for 48 h. For sectioning and contrasting, specimens were cut into semi-thin sections (1–2 microns), stained in Toluidine Blue and examined under a light microscope to select areas for analysis. The block was trimmed, ultrathin sections (60–70 nm) were cut in a Leica UCT Ultramictrotome and placed on a grid. The grids were contrasted in 5% uranylacetate and 3% Reynolds lead citrate for 10 and 2 min, respectively. Grids were examined by TEM (FEI Tecnai G2) operated at 80 kV. At least 20 vessels/mouse for a total of 3 mice/group were imaged and further analyzed.

2.6 | In vivo BBB permeability assay

Alexa Fluor-555 Cadaverine (11 μg/g; ThermoFisher Scientific, A30677) was injected into the tail vein of

wild-type and CD93$^{-/-}$ mice and let circulate for 2 h. After that, mice were anesthetized and perfused with PBS1x followed by 4% PFA. Brains and kidneys were excised and stored for further analysis. Successful injection of cadaverine was verified by examining kidneys of injected animals under a stereomicroscope (Leica, M205FA) equipped with DFC7000T lamp (Leica Microsystems). Brains were sectioned using a vibratome and processed for immunofluorescent staining. Tile-scans of brain coronal sections were obtained using a fluorescent microscope Leica DMi8 (20× objective, Leica Microsystems) and high magnification pictures of the vessels using a confocal microscope Leica SP8 (63× oil immersion objective). At least 4 tile-scans of brain coronal section/mouse for a total of 3 mice/group were imaged and further analyzed. A representative confocal image of at least 4 different brain areas/mouse for at least 3 mice/group is showed.

2.7 | Co-immunoprecipitation

Co-immunoprecipitation assays were performed using the Pierce co-immunoprecipitation kit (ThermoFisher Scientific, 26149) according to the manufacturer's instructions. Briefly, total protein extracts (300 µg) obtained from mouse lung lysates were immunoprecipitated with sheep anti-mouse CD93 antibody (10 µg; Cat# AF1696, RRID: AB_354937, R&D Systems). CD93$^{-/-}$ lung lysate was used as a negative control. Co-immunoprecipitated fraction and flow-through (unbound fraction) were blotted for anti-mouse VE-cadherin (Cat# 555289, RRID: AB_395707, BD Biosciences) and anti-mouse CD93 (Cat# AF1696, R&D Systems).

2.8 | Proximity ligation assay

Proximity ligation assay (PLA) was performed using the Duolink II kit (Cat# DUO92104, Sigma Aldrich, Missouri, USA) according to the manufacturer's instructions. Briefly, 4% PFA-fixed HDBECs were permeabilized with 0.1% Triton-X 100 in 3% BSA and blocked at 37°C during 1 h in blocking solution. Cells were incubated for 2 h with mouse anti-human CD93 (Cat# D198-3, MBL International) and rabbit anti-human VE-cadherin (Cat# 2500, Cell Signaling), Claudin-5 (Cat# 35-2500, ThermoFisher Scientific), or junctional adhesion molecule A (JAM-A)[16] primary antibodies followed by 30-min incubation at 37°C in ligation solution and 1-h incubation with PLA secondary probes. The PLA signal was amplified using Amplification Orange and Polymerase. Cells were washed in Buffer-B (Olink, Uppsala, Sweden), actin staining and nuclei detection were performed using Alexa 488 Phalloidin and Hoechst, respectively, and mounted for microscopy analysis using Fluoromount-G (Southern Biotech). Single primary antibodies with PLA probes and PLA probes without primary antibodies were routinely included as negative controls. Images were acquired under confocal microscope Leica SP8. The PLA signal was quantified in five different areas of the cell monolayer using the ImageJ software.

2.9 | siRNA transfections

HDBECs or HBMVECs were incubated with scrambled control siRNA or with a pool of two siRNAs against CD93 (Hs_CD93_1 and Hs_CD93_2; FlexiTube, Qiagen, Hilden, Germany) at a concentration of 2 nM in a mixture of 20% OptiMem (ThermoFisher Scientific) in EBM medium supplemented with 30 µL/mL Lipofectamine RNAiMAX (ThermoFisher Scientific). After 6 h, the medium was replaced with fresh medium and experiments were performed at days 2 and -3 after siRNA transfection.

2.10 | RhoGTPases pull-down activation assay

Levels of active RhoA, Rac1, and CDC42 were measured in total cell protein extract using RhoA/Rac1/Cdc42 Activation Assay Combo Biochem Kit (Cat# BK030; Cytoskeleton; Colorado, USA) according to the manufacturer's instructions. Briefly, CD93 siRNA or control siRNA-transfected HDBECs were grown until confluence and kept for 16 h in starvation medium (1% fetal bovine serum-endothelial basal medium (FBS-EBM)). Cells were harvested with the lysis buffer provided by the kit. Immediately after extraction, protein concentration was determined with a commercial assay (BCA Protein Assay Reagent kit, ThermoFisher Scientific) and equal amount of protein were incubated with GST-Rhotekin sepharose beads. The complete pulled down samples, containing only active proteins were re-suspended in NuPAGE LDS sample buffer and analyzed by western blot. Positive and negative controls provided by the kit were included in all experiments.

2.11 | Inhibition assay

Control or siRNA-transfected cells were grown until confluence, starved for 16 h with starvation medium containing EBM without growth factors and supplemented with 1% FBS. Cells were treated for 8 h with 10 µM of the ROCK inhibitor Y-27632 (Cat# 5.09228, Sigma-Aldrich) and

processed either by lysis and Western blot analysis or fixation in 4% PFA for immunofluorescent stainings. A representative blot images and immunofluorescent stainings of three independent experiments are shown.

2.12 | VE-cadherin internalization assay

VE-cadherin internalization was assessed by antibody-feeding assay.[19] Briefly, control or CD93 silenced confluent HDBECs were incubated with an antibody against VE-cadherin (Cat# MABT134; RRID: AB_10845943; Clone BV6; Merck, New Jersey, USA; 10 μg/mL) at 4°C for 1 h in EBM-MV2 containing 3% BSA without supplements. Unbound antibody was removed by washing cells in ice-cold EBM-MV2 medium. Cells were then cultured at 37°C for 4 h in the presence of 150 μM chloroquine (Cat# C6628, Sigma Aldrich) in EBM-MV2 medium with supplements followed by acid washing with PBS supplemented with Ca2+, Mg2+, 25 mM glycine, 3% BSA and adjusted to pH 2.7, to remove the antibody from cell surface. Cells were fixed with 2% PFA for 10 min at room temperature. Total VE-cadherin was stained with an antibody generated in another species (AF1002, R&D Systems). Samples were mounted with Fluoromount-G (Cat# 0100-01, Southern Biotech) and analyzed by confocal imaging. Representative images of immunofluorescent stainings of at least three different areas from three independent experiments are shown.

2.13 | Western blot

Protein lysates were diluted in NuPAGE LDS sample buffer under reducing condition and heated to 95°C for 5 min. The samples were separated onto a 4%–12% Bis-Tris gel in MOPS running buffer (ThermoFisher Scientific) and blotted onto a nitrocellulose membrane (Cat#15259794; Cytiva, Massachusetts, USA). The membranes were blocked with 5% BSA or 5% skimmed milk in Tris-buffered saline (TBS) with 0.05% Tween-20 and probed with VE-cadherin (Cat# 555289, BD Biosciences), CD93 (Cat# AF1696, R&D Systems), JAM-A (Cat# ab270446, Abcam), myosin light chain (MLC) phospho S20 (Cat# ab2480, Abcam, Cambridge, United Kingdom), total MLC (Cat# ab11082, Abcam), and β-actin (Cat# sc-1615, SantaCruz Biotechnology) primary antibodies followed by washing with 0.05% Tween-20/TBS and subsequent incubation with horseradish peroxidase-labeled secondary antibodies (Sigma Aldrich). Antibody binding was detected using the ECL Prime Western Blot detection kit (Cat# RPN2232, Cytiva) according to the manufacturer's instructions. Quantifications were performed using Image Lab software (ver 4, Bio-Rad). A representative blot image of at least three independent experiments is shown.

2.14 | RNA extraction and quantitative PCR

RNA from control or siRNA-treated HDBECs was extracted using the RNeasy Plus Mini Kit (Qiagen). Total RNA was transcribed using Superscript III reverse transcriptase in 20 μL total volume containing 250 ng of random hexamers and 40 units of RNase OUT inhibitor (ThermoFisher Scientific). mRNA expression of VE-cadherin and claudin-5 was quantified and normalized to HPRT by real-time PCR in duplicate reactions per sample with 0.25 μM forward (Fw) and reverse (Rs) primer in SYBR Green PCR Master Mix (ThermoFisher Scientific). Primer sequences: VEC-Fw: TTGGAACCAGATGC ACATTGAT; VEC-Rs: TCTTGCGACTCACGCTTGAC; CLDN5-Fw: CTCTGCTGGTTCGCCAACAT; CLDN5-Rs: CACAGACGGGTCGTAAAACTC; HPRT-Fw: CTTTG CTGACCTGCTGGATT; HPRT-Rs: TCCCCTGTTGACTG GTCATT.

2.15 | Image analysis

Image analysis was performed using the ImageJ (v.1.53q) software. For the analysis on the TEM images of brain vessels, at least 20 vessels each mouse, for a total of 3 mice per group were analyzed. Orientation of the endothelial cell junctions, identified as electron-dense linear structures between adjacent endothelial in brain vessels, was quantified in relation to the vessel lumen and classified as parallel oriented (angle between 0° and 45° towards the vessel lumen) or perpendicular oriented (angle between 90° and 45° towards the vessel lumen). Values represent the % of parallel and perpendicular oriented junctions normalized to the total junctions analyzed in each vessel. The number of membrane protrusions observed in the vessel lumen was manually counted and normalized to the vessel lumen perimeter. Analysis of immunofluorescent stainings was performed by selecting the positive signal of the protein of interest using a thresholding algorithm in ImageJ software. The positive area was then normalized to the number of cells in the field of view or to the respective vascular marker. Intercellular gaps in endothelial monolayer were quantified by manual thresholding the total cell-free area in the field of view and normalized by the cell number. Area and mean fluorescence intensity of extravasated cadaverine were measured in tile-scans of entire coronal sections from rostral, middle, and caudal brain regions of 3 mice per group. The cadaverine-positive

area was normalized by the total tissue area in each tile-scan. The cadaverine mean fluorescent intensity was measured within a ROI created by thresholding the cadaverine-positive area and corrected by subtracting the tissue background signal.

2.16 | Statistical analysis

Statistical analysis was performed using the GraphPad Prism V6.01 software (GraphPad Software, San CA, USA). Results are presented as mean ± standard error over the mean (SEM). Statistical differences between groups were analyzed using parametric test two-tailed *t*-student (when comparing two groups of values), one-way ANOVA (when comparing more than two groups of values), or two-way ANOVA (when two factors were involved). Multiple comparisons post hoc tests were chosen based on how many group comparisons were made (detailed post hoc test is specified in figure legends). Statistical significance is indicated as $*p < .05$, $**p < .01$, $***p < .001$, $****p < .0001$.

3 | RESULTS

3.1 | CD93 interacts with VE-cadherin and preserves the endothelial junction stability

To study the role of CD93 on endothelial barrier integrity in physiological conditions, we first asked whether CD93 directly interacts with the endothelial junction proteins VE-cadherin, claudin-5, and JAM-A. To this end, co-immunoprecipitation of CD93 interacting proteins using a monoclonal anti-CD93 antibody was performed in lung protein lysates of wild-type mice. Lungs were chosen due to the abundance of endothelial cells in this organ. As shown in Figure 1A, Western blot analysis of CD93-coimmunoprecipitated samples using antibodies directed against VE-cadherin, claudin-5, and JAM-A revealed a direct interaction between CD93 and VE-cadherin but not between CD93 and claudin-5 or CD93 and JAM-A. The interaction between VE-cadherin and CD93 was further corroborated in cultured human dermal blood endothelial cells (HDBECs) by in situ PLA technology, using oligonucleotide-linked antibodies. Positive PLA signals, indicating the presence of CD93-VE-cadherin complexes, were detected in control endothelial cells (green dots in Figure 1B; −VEGF). Interestingly, the interaction between CD93 and VE-cadherin was significantly reduced in response to VEGF treatment (green dots in Figure 1B, +VEGF). The specificity of the assay was confirmed by quantification of CD93-VE-cadherin PLA signals per cell (Figure 1C). The absence of interaction observed between CD93 and claudin-5 and CD93 and JAM-A in the lung protein lysate co-immunoprecipitation assay (Figure 1A) was further confirmed in HDBECs by in situ PLA (Figure S1A,B).

In line with our previous report showing an altered VE-cadherin pattern at the cell–cell junctions in response to CD93 downregulation,[10] immunofluorescent analysis of HDBECs after siRNA-mediated knockdown of CD93 showed a significant reduction of VE-cadherin in siCD93 cells as compared to the control cells (Figure 1D and quantification graph in Figure 1E). In addition, as shown in the high magnification images in Figure 1D, the reduction in VE-cadherin signal was predominantly observed at the cell–cell junctions. Interestingly, despite the absence of a direct interaction between CD93 and claudin-5, we observed a significant reduction in the claudin-5 level in the siCD93 cells as compared to the control condition (Figure 1F and quantification graph in Figure 1G). Although the claudin-5-positive signal was not homogeneously distributed at the cell junctions in the monolayer

FIGURE 1 CD93 interacts with VE-cadherin (VEC) and stabilizes endothelial junctions. (A) Western blot against VEC, Claudin 5 (Cldn5), and junctional adhesion molecule A (JAM-A) in CD93 co-immunoprecipitated lung protein lysates from wild-type and $CD93^{-/-}$ mice. CD93 co-immunoprecipitated fraction (IP:CD93) and unbound fraction (flow-through, FT:CD93). $CD93^{-/-}$ lung lysate was used as a negative control. (B) In situ proximity ligation assay (PLA) for CD93 and VEC in cultured human dermal blood endothelial cells (HDBECs) treated with or without VEGF. Positive signal (green dots) indicates proximity between CD93 and VEC. F-actin was visualized by phalloidin (red) and nuclei by Hoechst (blue). Scale bars: 20 μm. (C) Quantification of CD93 and VEC interactions per cell. The non-specific background signal was determined by PLA-negative controls as well as in CD93 siRNA-transfected HDBECs. $**p < .01$, $****p < .0001$, ns $p > .05$; One-way ANOVA with Tukey's multiple comparisons test. (D) VEC staining (green) in control (Mock, siCtrl) and CD93 siRNA-transfected HDBECs (siCD93_1, siCD93_2). Scale bars: 20 μm. (E) Quantification of VEC-positive area normalized to cell number in the field ($n = 3$ independent experiments). (F, G) Claudin-5 staining (Cldn5, green) and quantification graph, respectively ($n = 3$ independent experiments). $*p < .05$, $**p < .01$, $***p < .005$, ns $p > .05$; One-way ANOVA with Tukey's multiple comparisons test. High magnification images indicate VEC and Cldn5 signals at the cell–cell junctions (D and F respectively). (H) Intercellular gaps formation in control HDBECs (Mock and siCtrl) or silenced for CD93 (siCD93_1 and siCD93_2). Gaps between cells (light gray signal) were visualized by thresholding the cell-free area. (I) Quantification of the intercellular gaps area normalized to cell number in the field of view ($n = 3$ independent experiments). $****p < .0001$, $***p < .005$. ns $p > .05$; One-way ANOVA with Dunnett's multiple comparisons test.

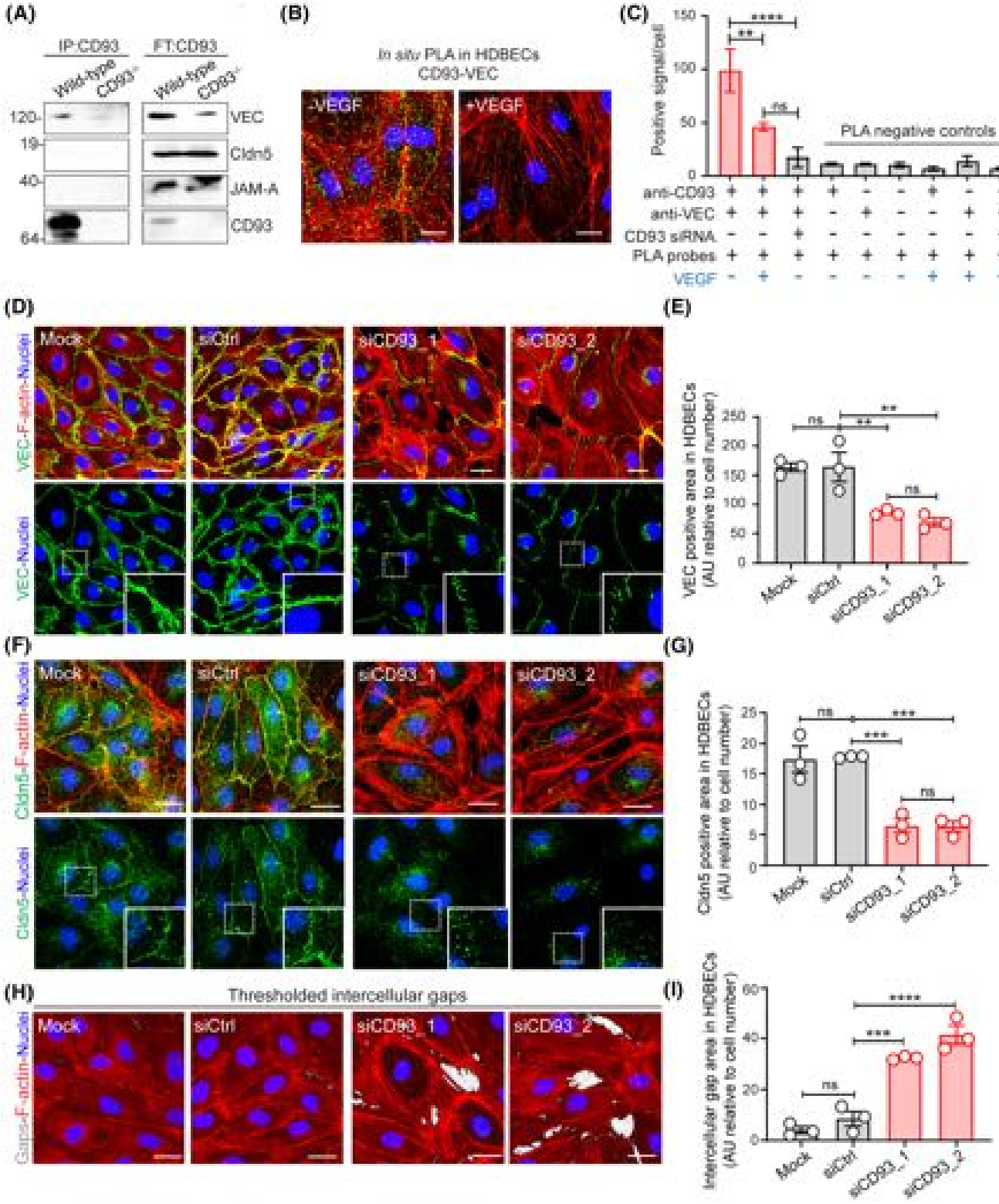

of control HDBECs, the signal was significantly lower or absent at the cell–cell junctions in siCD93 cells as shown in the high magnification images in Figure 1F.

Disengagement of VE-cadherin and claudin-5 from the cell junctions resulted in a disruption of the endothelial junction stability as indicated by the formation of intercellular gaps in confluent HDBECs after CD93 knockdown (Figure 1H,I).

Interestingly, VE-cadherin gene expression was similar in siCD93 HDBECs as compared to control cells (Figure S2A), suggesting that CD93 downregulation affects the stabilization of VE-cadherin at the cell–cell

junctions without interfering with the gene expression. In contrast, a significant reduction in claudin-5 mRNA levels was observed in siCD93 cells as compared to control cells (Figure S2B).

3.2 | CD93 regulates endothelial barrier properties through a Rho/Rho kinase-dependent pathway

RhoGTPases play a central role in regulating junction-associated actin dynamics and thus cell–cell adhesion.[17] We have previously shown that CD93 silencing is accompanied by strong stress fiber formation and weakened cell–cell contacts.[10] Moreover, recent studies have identified CD93 as a regulator of RhoGTPase signaling controlling cytoskeleton dynamics and cell adhesion and migration.[12,13] Therefore, to explore the molecular mechanism by which CD93 regulates the endothelial junction integrity, we investigated whether the compromised endothelial barrier function observed in response to CD93 deletion was mediated by RhoGTPases. The activity levels of RhoA, Rac1, and Cdc42 in endothelial cells after CD93 knockdown were assessed by an activation pull-down assay (Figure S3). In line with previous reports,[12,13] CD93 silencing in HDBECs produced a twofold increase in RhoA activity compared to the levels found in control cells. Concomitantly, levels of active Rac1 and Cdc42 were significantly reduced in siCD93 cells (Figure S3A and quantification graph in Figure S3B).

MLC is activated downstream RhoA and its effector Rho kinase (ROCK) (Figure 2A) and plays a key role in the contraction of actin stress fibers and cytoskeleton remodeling.[18] In agreement with enhanced activation of RhoA in response to CD93 downregulation, we observed a substantial increase in MLC phosphorylation (p-MLC) in endothelial cells treated with CD93 siRNA while the total MLC levels were unchanged (Figure 2B,C, −Y27632 group). This effect was rescued by treatment of cells with the ROCK inhibitor Y27632, which diminished p-MLC levels in siCD93 cells to control levels (Figure 2B,C, +Y27632 group). Moreover, the increase in actin stress fiber formation seen in response to CD93 downregulation was abolished in siCD93 cells treated with Y27632 inhibitor (Figure 2D and graph in Figure 2E).

In further agreement with the above observations of CD93 maintaining endothelial stability via RhoA/ROCK signaling, treatment of siCD93 cells with the Y27632 ROCK inhibitor restored the levels of VE-cadherin and claudin-5 to control levels (Figure 3A,C and Figure 3B,D respectively), and rescued their localization at the cell junctions (high magnification images of the junctions in Figure 3A,B). This resulted in a recovery of junction stability indicated by the closure of the intercellular gaps induced by CD93 downregulation (Figure 3E,F).

Due to the tight regulation of the endothelial cell junctions in the brain vasculature, the effect of CD93 downregulation on VE-cadherin and claudin-5 was further confirmed in HBMVECs (Figure S4). Similar to the destabilization of both junctional molecules observed in siCD93 HDBECs (Figures 1 and 3), downregulation of CD93 in HBMVECs (Figure S4A) resulted in a significant loss of VE-cadherin and claudin-5 signal and displacement of both molecules from the cell junctions (Figure S4B,D −Y27632 and Figure S4C,E −Y27632, respectively). This resulted in the disruption of the endothelial monolayer visualized by the formation of intercellular gaps in siCD93 HBMVECs (Figure S4F,G −Y27632). Inhibition of ROCK signaling in siCD93 HBMVECs rescued VE-cadherin and claudin-5 levels and their localization at cell-to-cell junctions compared to control conditions (Figure S4B–D +Y27632 and Figure S4C–E +Y27632), resulting in a complete recover of the endothelial monolayer integrity (Figure S4F,G +Y27632).

Taken together, these results suggest that CD93 controls actin dynamics and cell–cell junction remodeling through a Rho/ROCK-dependent signaling pathway.

3.3 | CD93 deficiency induces phosphorylation of VE-cadherin in vitro and promotes its internalization

Post-translational modifications of VE-cadherin, such as tyrosine phosphorylation, are known to be involved in the destabilization of the endothelial barrier and in the induction of vascular permeability.[19] Phosphorylation of VE-cadherin at Y658 (pY658) amino acid residue, important regulatory phosphorylation site that leads to disruption of the cell–cell junctions, was investigated by immunostaining in control and CD93 silenced HDBECs. Strikingly, siCD93 transfection significantly increased pY658 levels compared to the levels detected in control cells (Figure 4A, panel −Y27632 and graph in Figure 4B). Notably, inhibition of ROCK signaling by Y27632 inhibitor significantly reduced the pY658 levels in siCD93 cells to the levels comparable to control cells (Figure 4A, panel +Y27632 and graph in Figure 4B).

Phosphorylation of VE-cadherin has been shown to induce its internalization in vitro and in vivo, leading to increased vascular permeability.[15,20] Therefore, by employing an antibody-feeding assay, we assessed whether CD93 deficiency affects the VE-cadherin turnover in vitro.

Unfixed siCD93 and control HDBECs were incubated with anti-VE-cadherin antibody in the presence

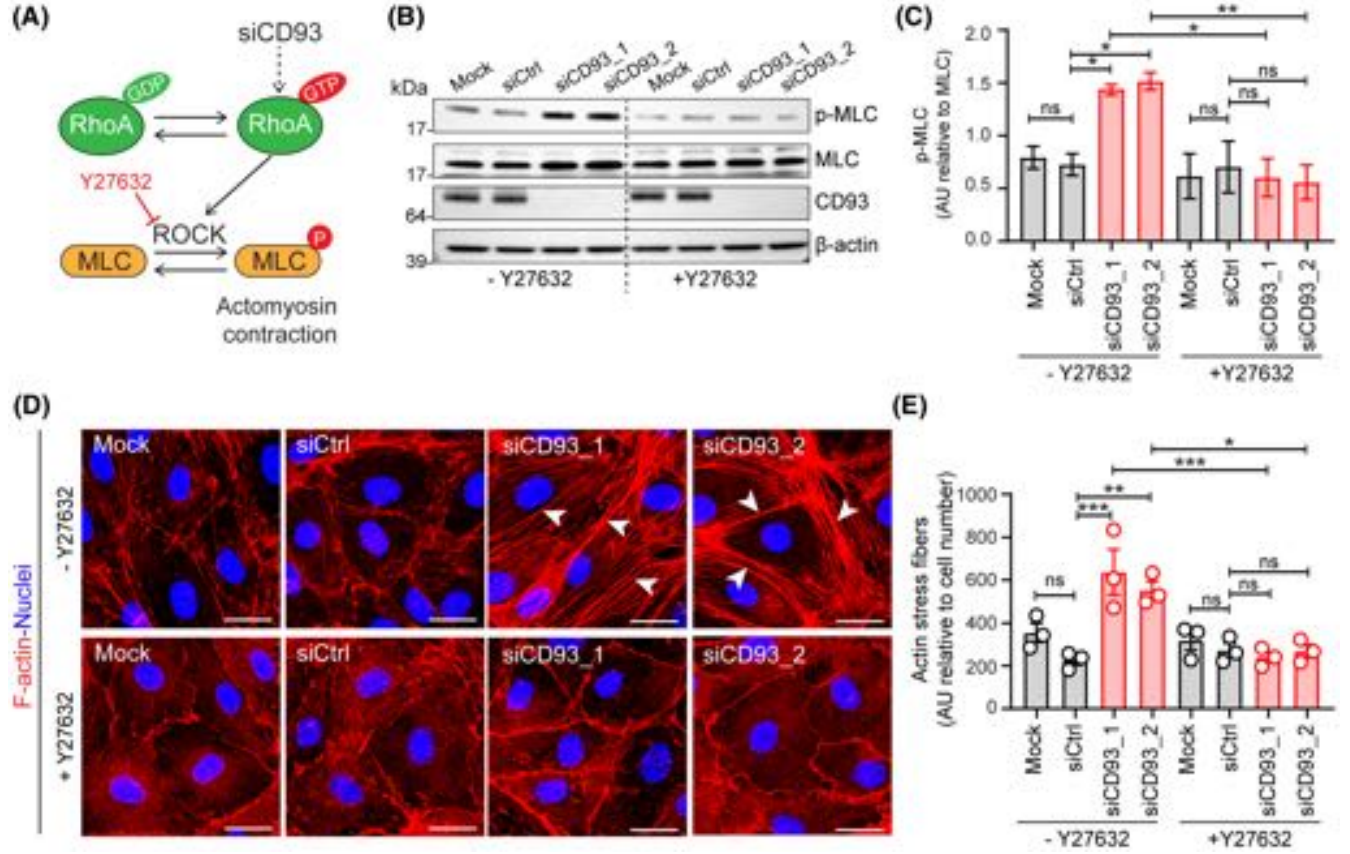

FIGURE 2 Inhibition of the Rho/ROCK signaling pathway rescues the increased actin stress fibers formation in CD93-deficient endothelial cells. (A) Schematic representation of CD93/RhoA-mediated myosin light chain (MLC) phosphorylation and inhibition of ROCK signaling through Y27632 inhibitor. (B) Western blot against Ser20 phosphorylated MLC (p-MLC), total MLC (MLC), CD93, and β-actin in control (Mock, siCtrl) or siCD93-transfected HDBECs (siCD93_1, siCD93_2) in the presence or absence of the ROCK inhibitor Y27632 (10 μM, 8 h). (C) Quantification of p-MLC normalized to total MLC ($n = 3$ independent experiments). $^{*}p < .05$, $^{**}p < .01$, ns $p > .05$; One-way ANOVA with Tukey's multiple comparisons test. (D) Immunofluorescent staining of F-actin (red) in control (Mock, siCtrl) and CD93 downregulated endothelial cells (siCD93_1, siCD93_2) in the presence or absence of the inhibitor Y27632 (arrowheads indicate stress fibers). Scale bar: 25 μm (E) Quantification of the actin stress fibers detected by F-actin staining and normalized to the number of cells per field of view ($n = 3$). $^{***}p < .005$, $^{**}p < .01$, $^{*}p < .05$, ns $p > .05$; One-way ANOVA with Tukey's multiple comparisons test.

of chloroquine, an inhibitor that prevents lysosomal degradation. Antibodies linked to cell surface-localized VE-cadherin were removed by acid washing, while antibodies bound to the internalized VE-cadherin could still be detected.[21] CD93 knockdown strongly increased the internalization of VE-cadherin compared to the control conditions. Indeed, co-staining with membrane-bound (green) and internalized (red) VE-cadherin showed that the disrupted membrane-bound VE-cadherin in siCD93 cells was accompanied by a significant increased amount of internalized VE-cadherin (arrowheads in Figure 4C and quantification graph in Figure 4D).

Altogether, these results show that loss of CD93 promotes VE-cadherin phosphorylation and endocytosis through a Rho/ROCK-dependent mechanism and indicate that CD93 expression is critical for stabilizing the endothelial cell–cell junctions.

3.4 | CD93 deletion induces endothelial junction remodeling in the brain vasculature

To determine the role CD93 in endothelial barrier function in vivo, we investigated the brain vasculature where vascular permeability is strictly regulated by the tight endothelial junctions of the blood–brain barrier.

We first examined the expression and distribution of the endothelial junction markers VE-cadherin and claudin-5 in vessels at the cerebral cortex region of 10-week-old CD93-deficient mice ($CD93^{-/-}$) and wild-type littermates. In line with the disruption of endothelial junctions observed in HDBECs and HBMVECs upon silencing of CD93, immunofluorescent staining of VE-cadherin in brain vessels of $CD93^{-/-}$ mice showed a disruption of VE-cadherin at the cell–cell contacts, indicated by a discontinuous staining pattern

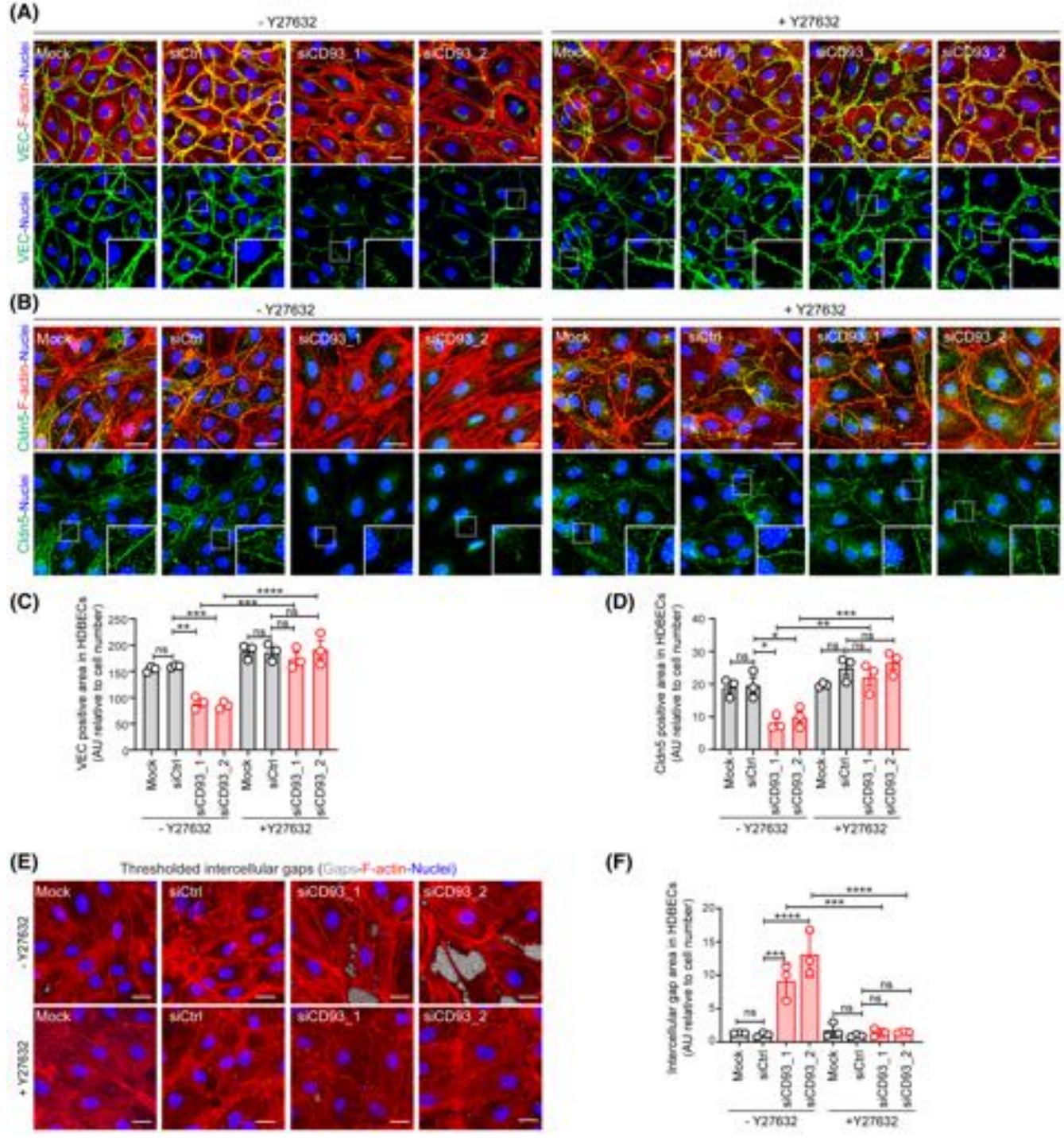

FIGURE 3 Junctions in CD93 downregulated endothelial cells are restored upon ROCK inhibition. (A) VE-cadherin (VEC) immunofluorescent staining (green) and F-actin (red) in control (Mock, siCtrl) and CD93 siRNA-transfected HDBEC (siCD93_1, siCD93_2) in the presence or absence of the ROCK inhibitor Y27632. Scale bars: 20 μm. (B) Immunofluorescent staining for claudin-5 (Cldn5, green) and F-actin (red) in the presence or absence of Y27632. Scale bars: 20 μm. High magnification images indicate VEC and Cldn5 signal al the cell–cell junctions (A and B respectively). (C, D) Quantification of VEC and Cldn5-positive area normalized to cell number ($n = 3$). ***$p < .005$, **$p < .01$, *$p < .05$, ns $p > .05$; One-way ANOVA with Tukey's multiple comparisons test. (E) Intercellular gaps formation (light gray) in control HDBEC monolayer (Mock and siCtrl) or silenced for CD93 (siCD93_1 and siCD93_2) in the presence or absence of Y27632. (F) Quantification of the intercellular gaps area normalized to cell number in the field of view ($n = 3$). ****$p < .0001$, ***$p < .005$. ns $p > .05$. One-way ANOVA with Tukey's multiple comparisons test.

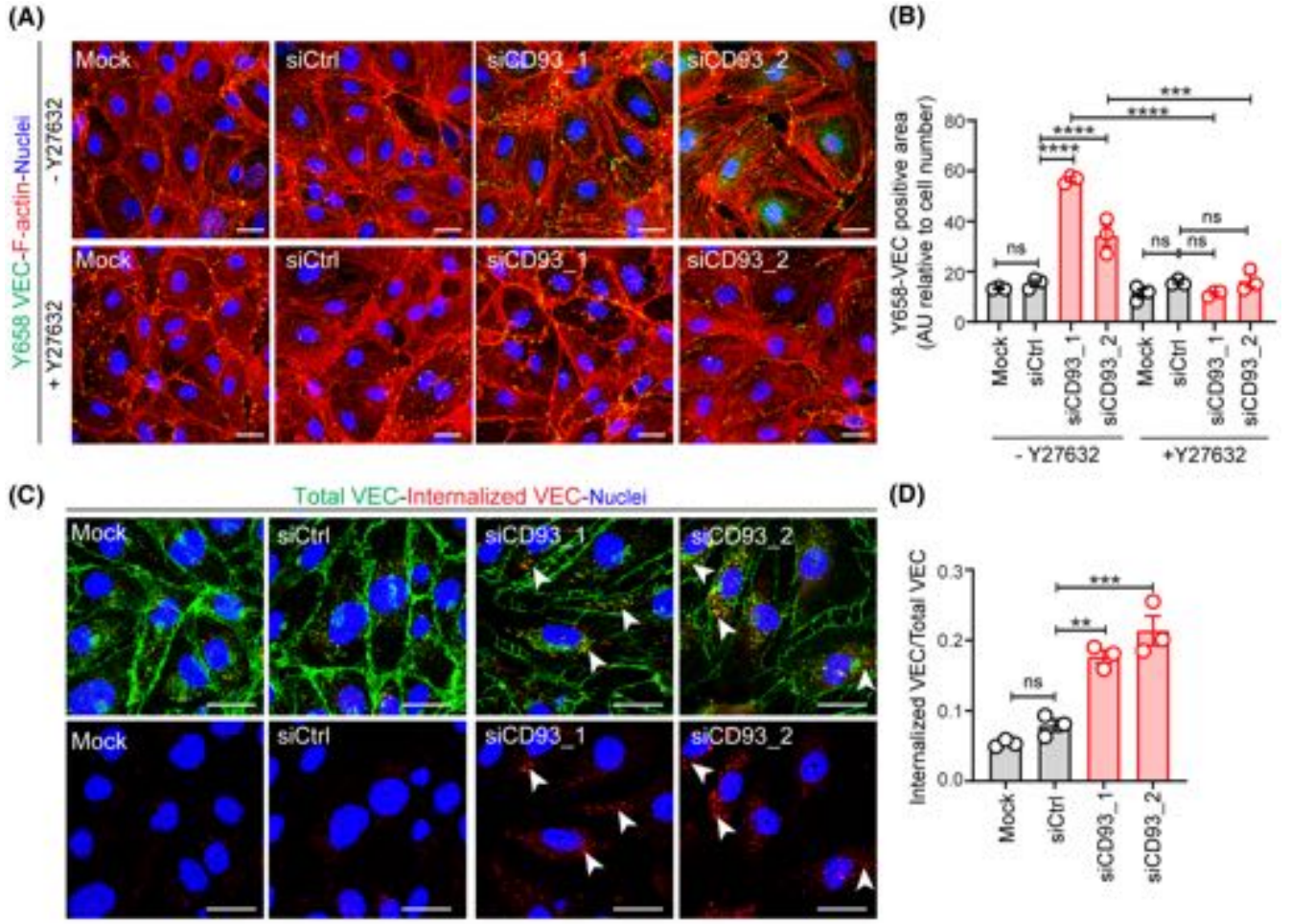

FIGURE 4 CD93 knockdown induces VE-cadherin (VEC) phosphorylation in a ROCK-dependent manner, causing its internalization. (A) Immunofluorescent staining of phosphorylated VEC tyrosine-658 (pY658-VEC; green) in control (Mock, siCtrl) or siCD93- (siCD93_1, siCD93_2) transfected HDBECs in the presence or absence of the inhibitor Y27632. Actin cytoskeleton is visualized by F-actin (red). Scale bars: 25 μm. (B) Quantification analysis of the pY568-VEC levels ($n = 3$ independent experiments). ****$p < .0001$, ***$p < .005$, ns $p > .05$, One-way ANOVA with Tukey's multiple comparisons test. (C) Antibody feeding assay showing internalized VEC (red, arrowheads) in control (Mock and siCtrl) and siCD93 (siCD93_1 and siCD93_2) HDBECs co-stained with total VEC (green) and nuclei (blue). Scale bars: 25 μm. (D) Quantification of internalized/total VEC in control and siCD93 cells ($n = 3$ independent experiments). ***$p < .005$, **$p < .01$, ns $p > .05$; One-way ANOVA with Tukey's multiple comparisons test.

(arrowheads in high magnification image, Figure 5A). In contrast, a homogeneous distribution of the VE-cadherin signal was observed in the wild-type mice (Figure 5A). Moreover, a significant general reduction in the VE-cadherin-positive signal was observed in the CD93$^{-/-}$ vessels as compared to the wild-type group (Figure 5B). Similarly, changes in the distribution and levels of the tight-junction protein claudin-5 were found in the CD93-deficient vessels (Figure 5C,D). Indeed, in contrast to the linear distribution of claudin-5 in endothelial junctions in the wild-type vessels, an intermittent staining pattern with a significant loss of the protein signal was observed in the CD93$^{-/-}$ group (arrowheads in high magnification image, Figure 5C and quantification graph in Figure 5D). In contrast, CD93 deficiency did not result in significant changes in the localization or levels of the intracellular scaffold protein ZO-1 in brain vessels (Figure S5A,B) or in cultured HDBECs (Figure S5C,D).

To determine whether the alteration of VE-Cadherin and claudin-5 in the brain vasculature of CD93-deficient mice was vessel type dependent, both molecules were co-stained together with arterial and venous markers (Figure S6). Homogeneous signal of VE-cadherin and claudin-5 was observed in arteries, identified by the positive staining for α-smooth muscle actin (ACTA2) and von Willebrand Factor (vWF), as well as in veins (vWF positive and ACTA2 negative) and capillaries (ACTA2 negative and vWF negative) of wild-type mice (Figure S6A,C respectively). Notably, the altered distribution patterns and reduced levels of VE-cadherin and claudin-5 in the CD93-deficient brain vasculature were observed to a similar extent in arteries, veins, and capillaries (arrowheads

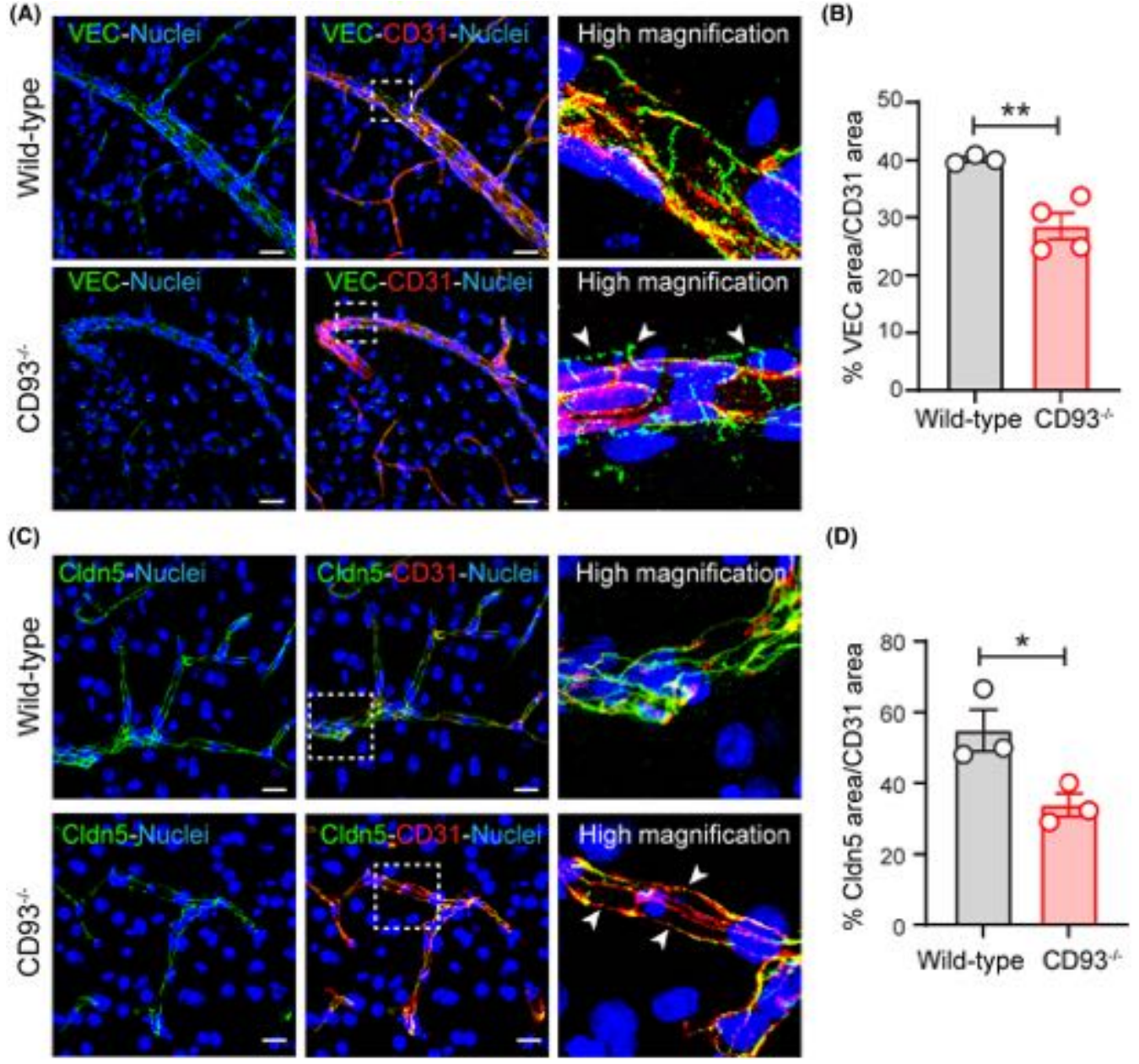

FIGURE 5 Loss of CD93 destabilizes brain endothelial cell–cell junctions. (A) Vascular immunofluorescent staining of VE-cadherin (VEC, green) in the brain cortex of wild-type and CD93$^{-/-}$. High magnification pictures show VEC expression pattern. Arrowheads in the CD93$^{-/-}$ group indicate irregular staining pattern. Scale bars: 20 μm. (B) Quantification of the VEC-positive signal in brain vessels of wild-type ($n = 3$) and CD93$^{-/-}$ ($n = 4$) mice. $^{**}p < .01$, two-tailed *t test*. (C) Claudin-5 immunofluorescent staining (Cldn5, green) in wild-type and CD93$^{-/-}$ brain vessels. Arrowheads in the high magnification image indicate loss of Cldn5 signal in the CD93$^{-/-}$ vessels. Scale bars: 20 μm. (D) Quantification of Cldn5-positive signal in the vessels of wild-type ($n = 3$) and CD93$^{-/-}$ ($n = 3$) mice. $^{*}p < .05$, two-tailed *t test*. Vessels are visualized by CD31 (red) and nuclei by Hoechst (blue).

in Figure S6B,D respectively) indicating a general effect of CD93 deficiency on the endothelial junctions of different vessel types.

The alteration in the distribution and levels of VE-cadherin and claudin-5 observed in CD93$^{-/-}$ vessels suggests remodeling of the junctions that might have consequences for their organization. Consistent with this, a morphological analysis of endothelial junctions, identified by TEM as electron-dense linear structures between adjacent endothelial cells (arrowheads in Figure 6A), revealed changes in the shape and orientation of these structures in CD93$^{-/-}$ vessels. Indeed, in wild-type mice, the majority of the endothelial junctions were arranged between overlapping flaps of adjacent endothelial cells, parallel to the vessel lumen displaying an elongated appearance (wild-type panel in

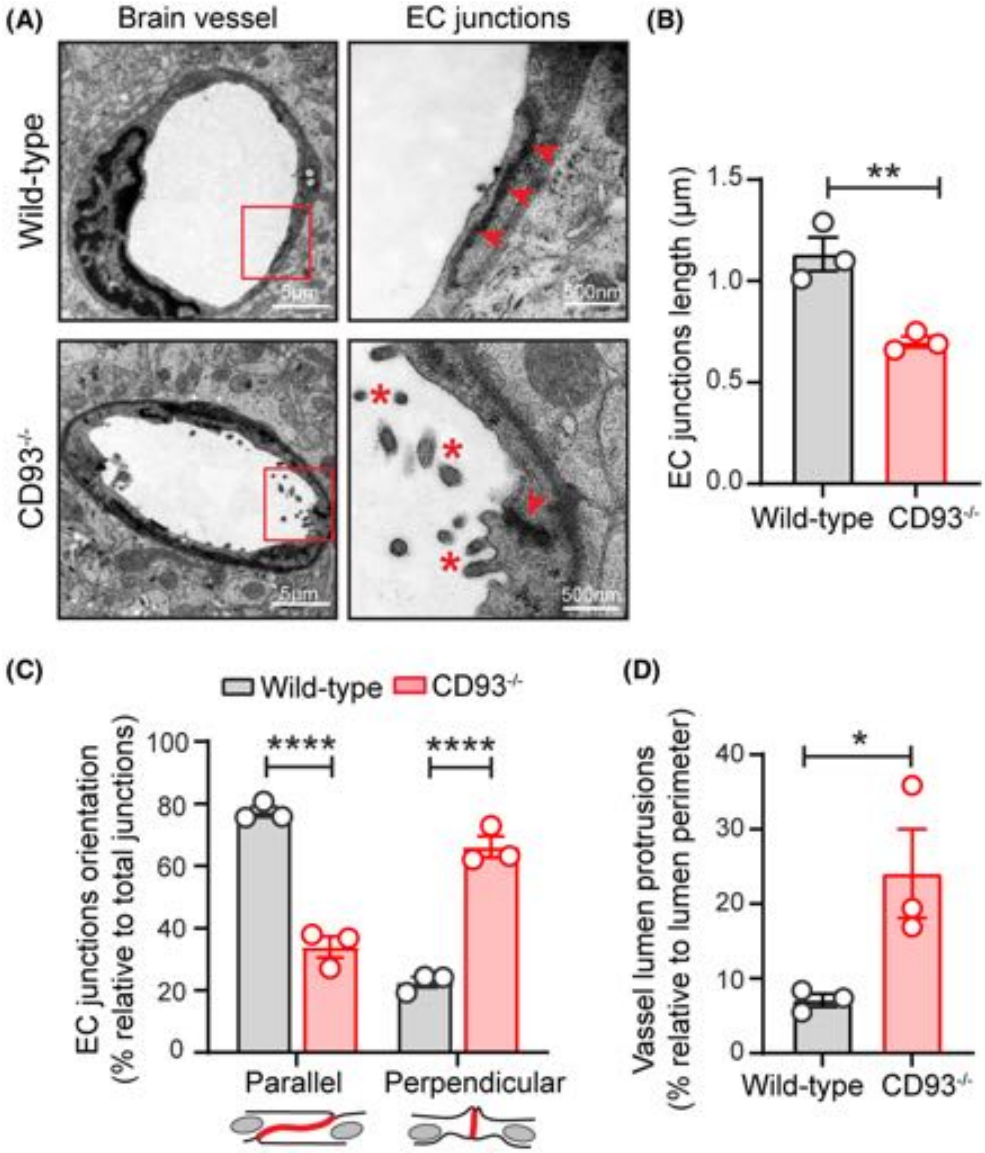

FIGURE 6 CD93 deletion induces morphological changes in the endothelial junctions of the brain vasculature. (A) Transmission electron microscopy showing brain vessels from wild-type and CD93$^{-/-}$ mice. Scale bars: 5 μm. High magnification images show the endothelial junctions (arrowheads) and membrane protrusions (asterisks). Scale bars: 500 nm. (B) Quantification of endothelial junction length in wild-type ($n = 3$) and CD93$^{-/-}$ ($n = 3$) mice. Values represent mean ± SEM of at least 20 vessels/mouse. $^{**}p < .01$, two-tailed *t test*. (C) Quantification of the endothelial junction orientation in relation to the vessel lumen in wild-type ($n = 3$) and CD93$^{-/-}$ ($n = 3$) mice. Values represent mean ± SEM of at least 20 vessels/mouse. $^{****}p < .0001$. Two-way ANOVA with Sidak's multi-comparisons test. (D) Quantification of the membrane protrusions in wild-type ($n = 3$) and CD93$^{-/-}$ ($n = 3$) mice. Values represent mean ± SEM of at least 20 vessels/mouse. $^{*}p < .05$, two-tailed *t test*.

Figure 6A). In contrast, CD93$^{-/-}$ brain vessels showed significantly shorter junctions perpendicularly oriented toward the vessel lumen (CD93$^{-/-}$ panel in Figure 6A and quantification of endothelial junctions length in Figure 6B). Quantification analysis of the junction orientation revealed that more than 65% of the junctions analyzed in CD93$^{-/-}$ brain vessels were perpendicularly oriented toward the vessel lumen, while 20% of the junctions displayed a similar orientation in wild-type mice (Figure 6C).

In addition to the altered length and orientation of the endothelial junctions observed in CD93$^{-/-}$ mice, analysis by TEM revealed an irregular vascular lumen in CD93-deficient vessels characterized by the presence of multiple luminal membrane protrusions (asterisks in Figure 6A), significantly higher in number as compared to those found in the wild-type vessels (Figure 6D). The vast majority of these luminal membrane protrusions were found in close proximity to the endothelial cell–cell contacts (Figure 6A), suggesting an increased rearrangement of the junctions in

response to CD93 deletion, likely contributing to barrier destabilization.

3.5 | CD93 deficiency induces phosphorylation of VE-cadherin in brain vessels and leads to increased BBB permeability in physiological conditions

To further investigate the function of CD93 in the stability of the endothelial junctions in vivo, we assessed the phosphorylation of VE-cadherin at Y658 (pY658) and Y685 (pY685) amino acid residues by immunostaining in CD93$^{-/-}$ mice or wild-type brain vessels. In accordance with the increased VE-cadherin phosphorylation observed in siCD93 HDBECs (Figure 4A,B), high levels of both pY658 and pY685 were found in the CD93-deficient vessels in contrast to the low levels found in the wild-type vessels (Figure 7A,B).

Quantification of the VE-cadherin phosphorylation showed that 54.6% ± 12.6% of the total VE-cadherin area in the analyzed brain vessels of CD93$^{-/-}$ mice stained positive for Y658 phosphorylation as compared to the 6.9% ± 2.1% detected in wild-type mice. Similarly, phosphorylation at Y685 was detected in 42.6% ± 3.8% of the total VE-cadherin area in CD93-deficient vessels and only 17.3% ± 3.9% in wild-type mice (graphs in Figure 7C,D).

To explore to which extent CD93 regulates BBB integrity, the 1KDa fluorescent tracer cadaverine-AlexaFluo-555 was administered intravenously in mice, followed by a 2-h circulation period. The accuracy of the cadaverine injection was confirmed by detecting the tracer signal in the kidneys of injected animals (Figure S7A). In accordance with the disturbed endothelial junctions, there was a modest but significant accumulation of the tracer in the brain tissue of CD93$^{-/-}$ mice (Figure 7E). Autofluorescence of brain tissue was assessed on uninjected mice (Figure S7B). Extravasated fluorescent tracer was detected in different parts of the analyzed coronal sections, including the cortex region (indicated by the number 1 in Figure 7F), as well as in the proximity of the midline between the hemispheres (indicated by the number 2 in Figure 7F) and in the ventral region of the brain (indicated by the number 3 in Figure 7F). Signal from extravasated cadaverine was observed throughout the entire brain in CD93$^{-/-}$ mice, and was most abundant in the middle and caudal regions (Figure 7E, quantification graphs in Figure 7G,H and Figure S7C).

The cadaverine extravasation was confirmed by confocal microscopy analysis showing the accumulation of the tracer in the perivascular tissue of CD93$^{-/-}$ mice (arrowheads in Figure 7I). In contrast, cadaverine did not extravasated in the brains of wild-type mice. The permeability of the BBB in CD93$^{-/-}$ mice was further assessed by analyzing the vascular leakage of high molecular weight molecules such as fibrinogen and endogenous IgG. Notably, both molecules were observed inside the blood vessels and there was no extravasation of either molecule in CD93-deficient mice (Figure S8A,B).

Taken together, loss of CD93 promotes VE-cadherin phosphorylation in the brain vessels, resulting in a dysregulation of endothelial junctions and an increased vascular leakage of a small molecular weight tracer.

4 | DISCUSSION

Increased vascular permeability and altered endothelial barrier properties greatly contribute to the severity of a wide range of pathological conditions including heart disease, cancer, stroke as well as psychiatric and neurodegenerative diseases.[22,23]

CD93 is increasingly recognized to play an important role in vascular biology and pathological angiogenesis.[24] Our previous studies in murine glioma[10,11] as well as studies on experimental peritonitis and autoimmune encephalomyelitis[25,26] suggest that CD93 affects vascular integrity during pathological conditions. However, its potential role in controlling the endothelial barrier functions in healthy individuals and the mechanisms involved have not been investigated prior to this study.

Here, we demonstrate that CD93 is required for stabilizing the endothelial cell–cell junctions and thereby contributes to the maintenance of the vascular integrity in physiological conditions. The remodeling of VE-cadherin and claudin-5 at the endothelial cell–cell junctions in response to CD93 deficiency promotes structural changes with junctions meeting end-to-end rather than forming overlapping flaps in brain vessels, leading to increased vascular permeability and leakage of small molecules in the mouse brain parenchyma. CD93 is expressed in the mouse vascular endothelium at embryonic day 9,[27] suggesting a role during vascular development. Therefore, it is tempting to hypothesize that the endothelial junction remodeling observed in response to CD93 deficiency might indicate that brain vessels fail to mature properly, leading to a defective blood–brain barrier.

Our data suggest that there are general defects in endothelial junctions in brain vessels of CD93 knockout mice. Indeed, remodeling of VE-cadherin and claudin-5 was observed to a similar extent in arteries, veins, and capillaries in CD93-deficient brains. This is consistent with an equal expression of CD93 in the endothelium of these vessel types in the brain.[28]

The contribution of endothelial barrier dysfunction to several disorders including psychiatric and

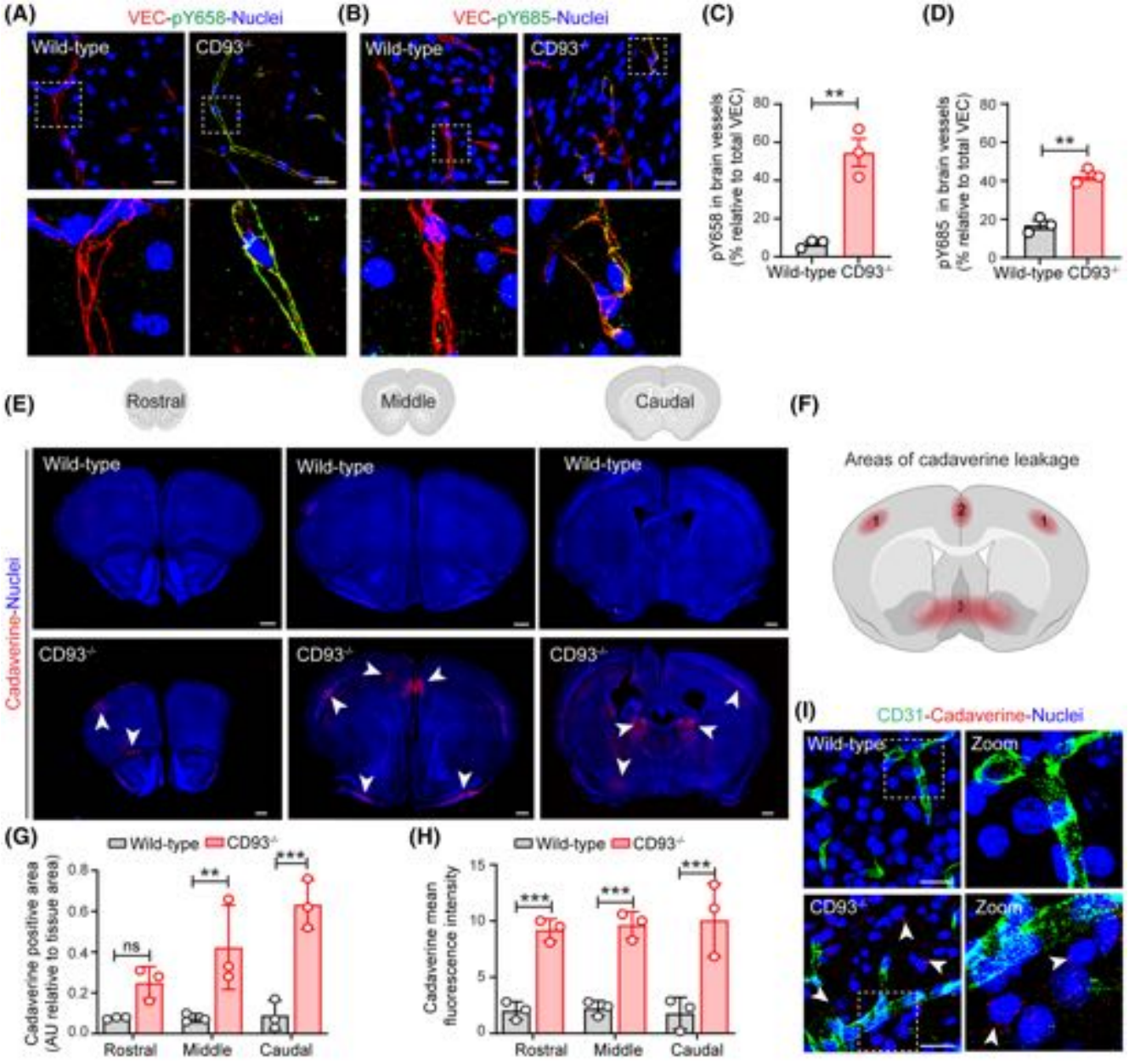

FIGURE 7 CD93 deficiency induces VE-cadherin phosphorylation at tyrosines Y658 and Y685 in vivo and impairs BBB function. (A–D) VE-cadherin (VEC) phosphorylation in brain vessels of wild-type and CD93$^{-/-}$ littermates. Immunostaining of pY658 VE-cadherin (green) (A), pY685 VE-cadherin (green) (B). Total VEC (VEC, red) and nuclei (Hoechst; blue). Scale bars: 20 μm. (C) Quantification of pY658-VEC relative to total-VEC in wild-type ($n = 3$) and CD93$^{-/-}$ ($n = 3$) mice. (D) Quantification of pY685-VEC relative to total-VEC in wild-type ($n = 3$) and CD93$^{-/-}$ ($n = 3$) mice. $^{**}p < .01$; two-tailed *t test*. (E–I) Analysis of blood–brain barrier permeability in mice injected intravenously with 1-kDa AlexaFluor-555 cadaverine. (E) Representative coronal sections of rostral, middle, and caudal brain regions assessed for extravasated cadaverine (red signal). Scale bars: 500 μm. (F) Schematic of a brain coronal section illustrating the areas where the cadaverine extravasation was observed (1 = cortex; 2 = midline between hemispheres; 3 = ventral region). Quantification of the cadaverine-positive area (G) and mean fluorescent intensity (H) in CD93$^{-/-}$ mice ($n = 3$) and wild-type mice ($n = 3$) after 2 h of circulation. $^{***}p < .005$, $^{**}p < .01$, ns $p > .05$; Two-way ANOVA with Sidak's multi-comparisons test. (I) Confocal images of brain vessels (CD31, green) and cadaverine tracer (red). Arrowheads indicate the extravasated tracer detected in CD93$^{-/-}$ group. Scale bars: 25 μm. Schematics were created with BioRender.com.

behavioral disorders[29] suggests a possible protective role for vascular CD93 in the development of neurological conditions. In accordance, the CD93 locus belongs to a set of genes associated with emotional empathy in children[30]; however, the role of CD93 in this trait remains to be further investigated. Moreover, a recent study demonstrated that CD93 deletion contributes to autism-like behavior in mice by disrupting the balance

between astrogenesis and neurogenesis in the late embryonic stage.[31]

Rac1 and Cdc42 are the main GTPases required for endothelial barrier maintenance and stabilization, whereas RhoA negatively regulates barrier properties by promoting MLC-dependent contraction of stress fibers via its effector Rho kinase (ROCK).[5] In line with this notion, our data indicate that CD93 promotes endothelial barrier stability by suppressing the activity of RhoA and inducing the activation of Rac1 and Cdc42. Indeed, junctional proteins that had been delocalized from endothelial junctions in response to CD93 depletion accumulated again at cell–cell contacts upon inhibition of ROCK signaling. This suggests that impaired organization of endothelial junctions in CD93-deficient cells was caused at least in part by an imbalance of myosin-generated subcellular tension downstream of RhoA activation.

In response to vascular permeability factors and blood flow, the tyrosine residues of VE-cadherin become phosphorylated at 685 and 658 sites through the action of Src family kinases followed by VE-cadherin internalization and vessel leakage.[15] Intriguingly, our findings indicate that vascular CD93 limits the phosphorylation of VE-cadherin at these tyrosine sites and maintains VE-cadherin at the junctions, protecting the integrity of the endothelial cell–cell contacts. However, a recent report demonstrated that CD93 downregulation inhibits Src phosphorylation during early cell adhesion,[13] suggesting that the increased phosphorylation of VE-cadherin observed in CD93$^{-/-}$ vessels, and in siCD93 endothelial cells may not be dependent on Src activity. The effect of CD93 on VE-cadherin phosphorylation may be explained by the physical interaction between the two molecules demonstrated by co-immunoprecipitation assay. Indeed, in response to the vascular permeability factor VEGF, the CD93-VE-cadherin complex was lost, suggesting that CD93 interacts with VE-cadherin in a constitutive manner at cell–cell junctions. Alternatively, the effect of CD93 on VE-cadherin stability at the cell–cell junctions might involve the regulation of vascular endothelial protein tyrosine phosphatase (VEPTP, PTPRB), a receptor type phosphatase that is crucial in the stabilization of endothelial junctions. Indeed, CD93 has been suggested to be a potential substrate of VEPTP,[32] and in quiescent endothelium VEPTP can stabilize VE-cadherin junctions by limiting RhoA signaling at the adherence junctions and reducing the VE-cadherin internalization rate.[33]

In summary, this study shows a key role of CD93 in the control of VE-cadherin phosphorylation, which has important implications for the stabilization of the endothelial junctions and maintenance of the vascular integrity. Thus, CD93 may be a potential target to be considered in the development of novel pharmaceutical interventions aimed at modulating vascular permeability.

AUTHOR CONTRIBUTIONS

Anna Dimberg and Roberta Lugano designed the research studies. Roberta Lugano, Kalyani Vemuri, and Stefano Barbera conducted the experiments. Roberta Lugano, Kalyani Vemuri, and Stefano Barbera acquired the data. Roberta Lugano, Kalyani Vemuri, and Anna Dimberg analyzed the data. Lena Claesson-Welsh and Elisabetta Dejana provided reagents and samples. Anna Dimberg and Roberta Lugano wrote the manuscript. Roberta Lugano, Kalyani Vemuri, Stefano Barbera, Maurizio Orlandini, Elisabetta Dejana, Lena Claesson-Welsh and Anna Dimberg edited and reviewed the manuscript.

ACKNOWLEDGMENTS

Assistance with Transmission Electron Microscopy analysis was provided by BioVis Core Facility/Electron microscopy at Department of Immunology, Genetics and Pathology, Uppsala University.

FUNDING INFORMATION

Swedish Cancer Society (CAN 2017/502, 20 1008 PjF, 20 1010 UsF). The Swedish Childhood Cancer Society (PR2018-0148, PR2021-0122). The Swedish Research Council (Dnr 2020-02563). Hjärnfonden (FO2022-0366). Knut and Alice Wallenberg Foundation (KAW 2019.0088).

DISCLOSURES

The authors declare no conflicts of interest.

DATA AVAILABILITY STATEMENT

The data that support the findings of this study are available in the methods and supplementary material of this article.

ORCID

Roberta Lugano https://orcid.org/0000-0002-7294-345X

REFERENCES

1. Claesson-Welsh L, Dejana E, McDonald DM. Permeability of the endothelial barrier: identifying and reconciling controversies. *Trends Mol Med*. 2021;27(4):314-331.
2. Stamatovic SM, Johnson AM, Keep RF, Andjelkovic AV. Junctional proteins of the blood-brain barrier: new insights into function and dysfunction. *Tissue Barriers*. 2016;4(1):e1154641.
3. Bravi L, Dejana E, Lampugnani MG. VE-cadherin at a glance. *Cell Tissue Res*. 2014;355(3):515-522.
4. Schnittler H, Taha M, Schnittler MO, Taha AA, Lindemann N, Seebach J. Actin filament dynamics and endothelial cell junctions: the Ying and Yang between stabilization and motion. *Cell Tissue Res*. 2014;355(3):529-543.
5. Spindler V, Schlegel N, Waschke J. Role of GTPases in control of microvascular permeability. *Cardiovasc Res*. 2010;87(2):243-253.
6. Kugelmann D, Rotkopf LT, Radeva MY, Garcia-Ponce A, Walter E, Waschke J. Histamine causes endothelial barrier disruption

via Ca(2+)-mediated RhoA activation and tension at adherens junctions. *Sci Rep*. 2018;8(1):13229.
7. Dieterich LC, Mellberg S, Langenkamp E, et al. Transcriptional profiling of human glioblastoma vessels indicates a key role of VEGF-A and TGFbeta2 in vascular abnormalization. *J Pathol*. 2012;228:378-390.
8. Masiero M, Simões FC, Han HD, et al. A core human primary tumor angiogenesis signature identifies the endothelial orphan receptor ELTD1 as a key regulator of angiogenesis. *Cancer Cell*. 2013;24(2):229-241.
9. Zhang M, Bohlson SS, Dy M, Tenner AJ. Modulated interaction of the ERM protein, moesin, with CD93. *Immunology*. 2005;115(1):63-73.
10. Langenkamp E, Zhang L, Lugano R, et al. Elevated expression of the C-type lectin CD93 in the glioblastoma vasculature regulates cytoskeletal rearrangements that enhance vessel function and reduce host survival. *Cancer Res*. 2015;75(21):4504-4516.
11. Lugano R, Vemuri K, Yu D, et al. CD93 promotes beta1 integrin activation and fibronectin fibrillogenesis during tumor angiogenesis. *J Clin Invest*. 2018;128(8):3280-3297.
12. Barbera S, Lugano R, Pedalina A, et al. The C-type lectin CD93 controls endothelial cell migration via activation of the Rho family of small GTPases. *Matrix Biol*. 2021;99:1-17.
13. Barbera S, Raucci L, Lugano R, et al. CD93 signaling via rho proteins drives cytoskeletal remodeling in spreading endothelial cells. *Int J Mol Sci*. 2021;22(22):12417.
14. Norsworthy PJ, Fossati-Jimack L, Cortes-Hernandez J, et al. Murine CD93 (C1qRp) contributes to the removal of apoptotic cells in vivo but is not required for C1q-mediated enhancement of phagocytosis. *J Immunol*. 2004;172(6):3406-3414.
15. Orsenigo F, Giampietro C, Ferrari A, et al. Phosphorylation of VE-cadherin is modulated by haemodynamic forces and contributes to the regulation of vascular permeability in vivo. *Nat Commun*. 2012;3:1208.
16. Giannotta M, Benedetti S, Tedesco FS, et al. Targeting endothelial junctional adhesion molecule-A/EPAC/Rap-1 axis as a novel strategy to increase stem cell engraftment in dystrophic muscles. *EMBO Mol Med*. 2014;6(2):239-258.
17. Timmerman I, Heemskerk N, Kroon J, et al. A local VE-cadherin and Trio-based signaling complex stabilizes endothelial junctions through Rac1. *J Cell Sci*. 2015;128(16):3041-3054.
18. Katoh K, Kano Y, Noda Y. Rho-associated kinase-dependent contraction of stress fibres and the organization of focal adhesions. *J R Soc Interface*. 2011;8(56):305-311.
19. Wessel F, Winderlich M, Holm M, et al. Leukocyte extravasation and vascular permeability are each controlled in vivo by different tyrosine residues of VE-cadherin. *Nat Immunol*. 2014;15(3):223-230.
20. Gavard J, Gutkind JS. VEGF controls endothelial-cell permeability by promoting the beta-arrestin-dependent endocytosis of VE-cadherin. *Nat Cell Biol*. 2006;8(11):1223-1234.
21. Xiao K, Allison DF, Buckley KM, et al. Cellular levels of p120 catenin function as a set point for cadherin expression levels in microvascular endothelial cells. *J Cell Biol*. 2003;163(3):535-545.
22. Profaci CP, Munji RN, Pulido RS, Daneman R. The blood-brain barrier in health and disease: important unanswered questions. *J Exp Med*. 2020;217(4):e20190062.
23. Park-Windhol C, D'Amore PA. Disorders of vascular permeability. *Annu Rev Pathol*. 2016;11:251-281.
24. Khan KA, McMurray JL, Mohammed F, Bicknell R. C-type lectin domain group 14 proteins in vascular biology, cancer and inflammation. *FEBS J*. 2019;286(17):3299-3332.
25. Greenlee-Wacker MC, Briseño C, Galvan M, Moriel G, Velázquez P, Bohlson SS. Membrane-associated CD93 regulates leukocyte migration and C1q-hemolytic activity during murine peritonitis. *J Immunol*. 2011;187(6):3353-3361.
26. Griffiths MR, Botto M, Morgan BP, Neal JW, Gasque P. CD93 regulates central nervous system inflammation in two mouse models of autoimmune encephalomyelitis. *Immunology*. 2018;155(3):346-355.
27. Petrenko O, Beavis A, Klaine M, Kittappa R, Godin I, Lemischka IR. The molecular characterization of the fetal stem cell marker AA4. *Immunity*. 1999;10(6):691-700.
28. Vanlandewijck M, He L, Mäe MA, et al. A molecular atlas of cell types and zonation in the brain vasculature. *Nature*. 2018;554(7693):475-480.
29. Kealy J, Greene C, Campbell M. Blood-brain barrier regulation in psychiatric disorders. *Neurosci Lett*. 2020;726:133664.
30. Woodbury-Smith MR, Paterson AD, Szatmari P, Scherer SW. Genome-wide association study of emotional empathy in children. *Sci Rep*. 2020;10(1):7469.
31. Liang Q, Su L, Zhang D, Jiao J. CD93 negatively regulates astrogenesis in response to MMRN2 through the transcriptional repressor ZFP503 in the developing brain. *Proc Natl Acad Sci U S A*. 2020;117(17):9413-9422.
32. Drexler HCA, Vockel M, Polaschegg C, Frye M, Peters K, Vestweber D. Vascular endothelial receptor tyrosine phosphatase: identification of novel substrates related to junctions and a ternary complex with EPHB4 and TIE2. *Mol Cell Proteomics*. 2019;18(10):2058-2077.
33. Juettner VV, Kruse K, Dan A, et al. VE-PTP stabilizes VE-cadherin junctions and the endothelial barrier via a phosphatase-independent mechanism. *J Cell Biol*. 2019;218(5):1725-1742.

SUPPORTING INFORMATION

Additional supporting information can be found online in the Supporting Information section at the end of this article.

How to cite this article: Lugano R, Vemuri K, Barbera S, et al. CD93 maintains endothelial barrier function by limiting the phosphorylation and turnover of VE-cadherin. *The FASEB Journal*. 2023;37:e22894. doi:10.1096/fj.202201623RR